Direct mapping of the lateral force gradient on Si(111)-7×7

Shigeki Kawai,[1,2,*] Naruo Sasaki,[3] and Hideki Kawakatsu[1]
[1]*Institute of Industrial Science, The University of Tokyo, Komaba 4-6-1, Meguro-ku, Tokyo 153-8505, Japan and CREST, Japan Science and Technology Agency, Hon-machi 4-1-8, Kawaguchi, Saitama 332-0012, Japan*
[2]*Department of Physics, University of Basel, Klingelbergstr. 82, 4056 Basel, Switzerland*
[3]*Department of Materials and Life Science, Faculty of Science and Technology, Seikei University, Kitamachi 3-3-1, Kichijoji, Musashino-shi, Tokyo 180-8633, Japan*
(Received 9 December 2008; revised manuscript received 16 March 2009; published 13 May 2009)

Lateral force gradient of down to 0.01 N/m on Si(111)-7×7 was directly detected by dynamic lateral-force microscopy with an amplitude of 81 pm. Positive and negative torsional resonance frequency shifts of a silicon cantilever caused by the attractive interaction inward and outward tip ditherings were detected on adatom and nonadatom sites, respectively. The lateral force of down to subpiconewton was measurable with direct lateral-force spectroscopy. The converted lateral force predicts a possibility of the stick-slip motion in the noncontact region. The theoretical calculations were in good qualitative agreement with the experiments.

DOI: 10.1103/PhysRevB.79.195412 PACS number(s): 68.35.Af, 07.79.Sp, 34.20.Cf

I. INTRODUCTION

In 1995, an atomically resolved imaging was demonstrated by frequency modulation-dynamic mode atomic force microscopy (DFM).[1] The vertical interaction force gradient, which is the second derivative of the potential in the vertical direction, changes the resonance frequency of a cantilever and the frequency shift is used to regulate the tip-sample distance.[2] The potential between tip and sample also distributes in the horizontal direction, raising the atomic lateral force. However, most of the actual solid surfaces are rough, at least on a microscopic scale, and measured lateral forces are mainly caused by mechanical deformations at the large contact area.[3] Friction/lateral-force microscopy (LFM) (Ref. 4) has succeeded in reducing the contact area of down to several nm^2 and has enabled nanotribology studies while avoiding the large deformations.[5–7] Nevertheless, the contact is of a multiasperity nature and atomic-scale deformations of tip and sample usually happen.[8] Moreover, since a soft cantilever is used, instabilities of the cantilever motion, the so-called stick-slip motion, are usually caused and the actual lateral interaction between tip and sample is not easily detectable.

Recently, attempts to directly detect the atomic lateral interaction were demonstrated with dynamic LFM (DLFM).[9–11] In DLFM, the tip was being dithered parallel to the surface and the lateral force gradient was detected via the frequency shift. Since the detection is based on the frequency modulation technique,[2] a stiff cantilever can be used while keeping a high sensitivity. Therefore, the stick-slip motion can be avoided. Moreover, the high sensitivity enables detections far from the surface and the deformations of tip and sample can be minimized. So far atomic contrast of Si(111)-7×7 was obtained with this method.[10,11] On the other hand, indirectly the lateral force can be obtained by differentiating the potential, which is converted from experimentally detected two-dimensional vertical-distance-dependence measurements in the lateral direction.[12–14] Since this approach includes numerical deviations the noise in the measured frequency shift is enhanced and the detection sensitivity would decline. Furthermore, setting the tip closer to the sample surface increases the sensitivity but the atomic-scale deformations of tip and sample would become larger. In fact, the influence of the deformations to the converted potential is not clear.[15]

Figure 1(a) shows the schematic drawing of Si(111)-7×7.[16] The *XYZ* axes are defined hereafter. Figure 1(b) shows the calculated potential map along the longitudinal diagonal of the unit cell with the Morse potential.[17,18] The first and second derivatives of the potential in the *X* direction give the lateral force and the lateral force gradient as shown in Figs. 1(c) and 1(d), respectively. Positive- and negative-force gradients are observed around each adatom even with the attractive interaction and the distance dependence of the lateral gradient in DLFM is stronger than that of the vertical-force

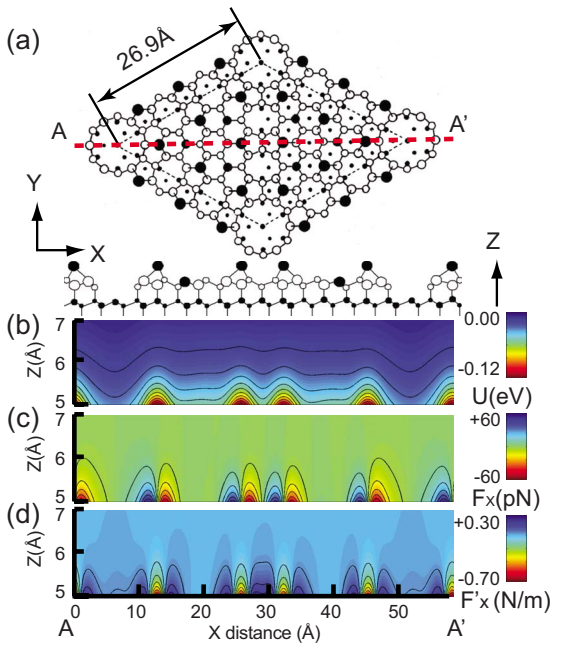

FIG. 1. (Color online) (a) Schematic drawing of Si(111)-7×7. Simulated (b) potential map $U(X,Z)$, (c) lateral-force map $F_X(X,Z)$, and (d) lateral-force-gradient map $F'_X(X,Z)$ in the *X* direction.

gradient in conventional DFM. Once the force gradient on the flat surface is averaged over a large amplitude, the lateral-force conversion via the measured frequency shift becomes impossible. Therefore, the direct-force gradient detection with an ultrasmall amplitude operation is an imperative technique. So far the lateral-force conversion by direct DLFM has been demonstrated only at an atomic step where the influence of the amplitude is less.[9]

Here we demonstrate a quantitative lateral-force-gradient field mapping on Si(111)-7×7. The lateral force gradient and its converted lateral force could be atomically resolved with resolutions of below 0.01 N/pm and 1 pN, respectively. The theoretical calculation was in good agreement with the experimental results.

II. EXPERIMENTAL

The experiment was performed with a homemade ultrahigh-vacuum DFM operating at room temperature (RT).[19] The torsional resonance mode of a Si cantilever (Nanosensor NCH-SSS) was used to detect the interaction between tip and sample. The high mechanical quality factor Q_{TR} of 110 810 with the high resonance frequency f_{TR} of 2.2 MHz enhanced the detection limit[2] and the high stiffness k_{TR} of 1250 N/m enabled a stable ultrasmall amplitude operation.[20,21] The tip was cleaned by Ar^+ sputtering (t =30 min, $P_{Ar}=1.0\times10^{-5}$ Pa, $I_{ion}<0.1$ μA, and U_{ex} =610 eV) after removing water layers by baking at 150 °C. The sample of Si(111)-7×7 was prepared *in situ* by dc heating at 1200 °C. The tip-sample distance, which had unavoidable thermal drifts at RT, was regulated with a constant time-averaged tunneling current. The tunneling regulation is desirable for this measurement because the tip-sample distance can be set larger than that in DFM, especially in the case of the Si surface with a bias voltage of above 1.5 V, and hence the deformations of tip and sample can be minimized. The dithering amplitude A_{dith} was directly calibrated with amplitude-induced artifacts, appearing in scanning tunneling microscopy (STM) topographies.[22] When a peak-to-peak amplitude was fitted to the neighboring adatom gap a single protrusion appeared at the middle of the gap due to the time-averaged tunneling regulation.

III. RESULTS AND DISCUSSION

Figure 2(a) shows the atomically resolved frequency-shift Δf_{TR} map at a constant tunneling resistance of 3 GΩ. The fast-scan direction was the X direction. Since the dithering direction of the tip was the Y direction, the detected frequency shift can be regarded as a time-averaged force gradient in the Y direction. All of the adatoms could be clearly resolved and were observed to have oval-shaped features with a long diagonal perpendicular to the dithering direction. The dithering amplitude of 81 pm was so small that the distortion in the STM topographic map was negligibly small [Fig. 2(b)]. Since another image obtained with a scan direction rotated by 90° [Fig. 2(c)] and a simulated image [Fig. 2(e)] show just the same pattern as Fig. 2(a), this shape of the contrast was not due to the artifact of the fast scan. Positive

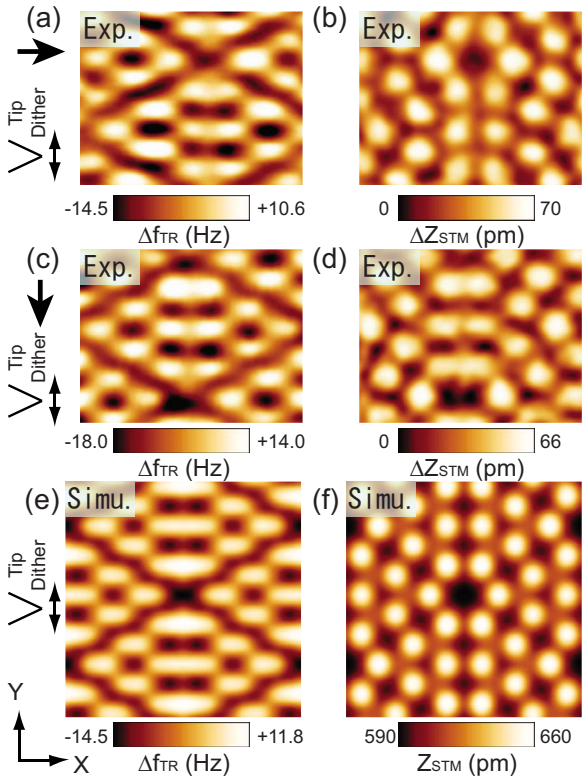

FIG. 2. (Color online) (a) Experimentally obtained frequency shift map and (b) STM topographic map with a fast scan direction of X. (c) Experimentally obtained frequency-shift map and (d) STM topographic map with a fast scan direction of Y. (e) Simulated-frequency map and (f) STM topographic map. Arrow shows the direction of the fast scan. Imaging and simulation parameters; f_{TR} =2.216275 MHz, Q_{TR}=110810, A_{dith}=81 pm, $\bar{I}_t$=0.6 nA, and V_{bias}=1.8 V.

and negative frequency shifts were detected at the adatom and nonadatom sites, respectively. It is worth noting that no significant change in the frequency shift was detected by changing the sample bias voltage. The long-range electrostatic force dependent on the bias voltage is non-site dependent and homogeneously decreases with the tip-sample distance. Therefore, when the tip is being dithered perfectly parallel to the sample surface, the long-range interaction does not affect the lateral-force-gradient measurement. It means that only the site-dependent short-range interaction, arising from the Si-Si covalent bonding, contributed to the lateral interaction on the flat terrace. Figures 2(e) and 2(f) show simulated frequency shift and STM topographic maps, respectively. In order to adjust to the detection direction in the experiment, the lateral force was calculated by deviating the potential in the Y direction. The calculation of the tunneling current was based on the independent-state model[23] where the tunneling-matrix elements between tip p_z state and individual surface p_z states contribute to the tunneling current. The position of the adatoms, which is calculated with the first-principles theory, was used.[24] The calculation parameters were the same as those used in the experiment. First, the STM topographic map was numerically calculated by

$$\bar{I}_t = \frac{1}{2\pi}\int_0^{2\pi} I_t(Y + A_{\text{dith}} \cos\theta)d\theta = 0.6 \text{ nA}. \quad (1)$$

The parameters in the calculation of the tunneling current were carefully adjusted to obtain the corrugation amplitude of 70 pm. Next, the frequency shift map, corresponding to the simulated STM topographic map, was numerically obtained as[25]

$$\Delta f_{\text{TR}} = -\frac{f_{\text{TR}}}{2\pi A_{\text{dith}} k_{\text{TR}}}\int_0^{2\pi} F_Y(Y + A_{\text{dith}} \cos\theta)\cos\theta d\theta. \quad (2)$$

Due to the anisotropic lateral-force-gradient detection, the adatoms are observed to be elliptical. As can be seen, Fig. 2(e) is in good agreement with Figs. 2(a) and 2(c). The tip-sample distance evaluated from the tunneling resistance was in the range of 5.9–6.6 Å (the attractive interaction-force region) and the tip was located 1–2 Å farther from the surface than the tip in vertical DFM.[18] The positive and negative frequency shifts were thus caused by the inward and outward directions of the attractive force with respect to the center of the dithering. The lateral interaction force at the distance (Z=5.9–6.6 Å) was found to be around ±5 pN in Fig. 1(c). Furthermore, the simulated maps of the frequency shift [Fig. 2(e)] and the tunneling current [Fig. 2(f)] obtained by the rigid tip-surface model are qualitatively in good agreement with the experimental ones as shown in Fig. 2. Therefore, deformations of the tip apex and the adatoms of Si(111)-7 ×7 are negligible in the present work.

A series of 17 frequency-shift maps with $\bar{I}_t$=0.1 ~1.0 nA was obtained. Figure 3(a) shows one example obtained with $\bar{I}_t$=1.0 nA. The contour plot indicates the positions with zero frequency shift. By extracting line profiles from each frequency-shift maps along A-A' the two-dimensional frequency shift map in the X-Z plane was reconstructed as shown in Fig. 3(b). The tip-sample distance was normalized with $Z_{\text{nor}} = -\ln(\bar{I}_t/1.0 \text{ nA})$. Since all images were obtained in the attractive regime, the variation of the time-averaged lateral force gradient was simply decreased with increasing the tip-sample distance. The neutral X positions with zero frequency shift stay constant at any tip-sample distance in the measured range. The time-average force gradient was calculated by $\bar{F}'_Y = -2k_{\text{TR}}\Delta f_{\text{TR}}/f_{\text{TR}}$ and reached below 0.01 N/pm while keeping atomic resolution.

Figure 4(a) shows the line profile as the same position as along B-B' in Fig. 3(a). The tip-sample distance was larger than in Fig. 3(a) ($\bar{I}_t$=0.25 nA). As can be seen, a periodic frequency shift curve was obtained. Since the line profile along the Y direction was extracted from the lateral-force-gradient map in the same Y direction, the lateral force conversion is possible. In order to convert to the force, the position with F_Y=0 has to be first defined. In the vertical-force conversion, the position can be simply set far from the surface.[15] On the other hand, the lateral-force conversion is not simple. However, since we have the periodic frequency-shift curve and since the position with $\bar{F}'_Y$=0 is independent

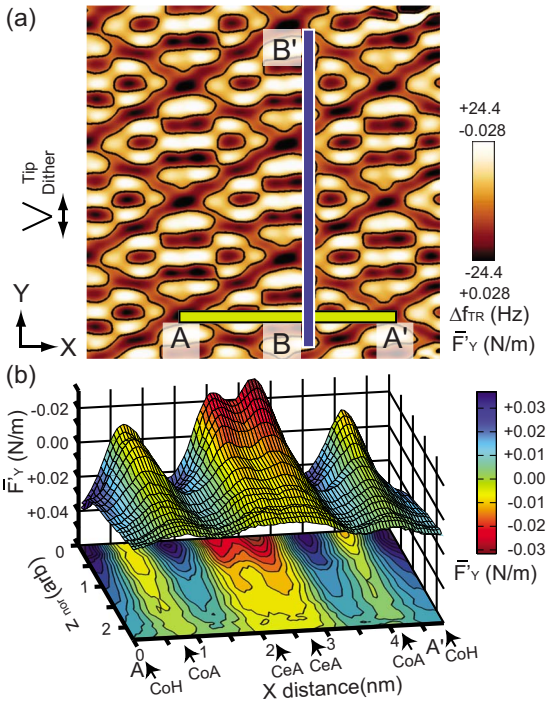

FIG. 3. (Color online) (a) $\bar{F}'_Y(X,Y)$ map. Solid lines show the positions with $\bar{F}'_Y$=0 N/m for $\bar{I}_t$=1.0 nA. (b) $\bar{F}'_Y(X,Z)$ map along A-A'. $\bar{I}_t$=0.1 ~1.0 nA and V_{bias}=1.8 V. CoH is the corner hole and CoA and CeA are the corner and center adatoms, respectively.

of the tip-sample distance as shown in Fig. 3(b), the position with zero frequency shift presumably equals to that with F_Y=0. Here the lateral-force conversion is performed with $F(Y) = \int_{Y_{F_Y=0}}^{Y} -2k_{\text{TR}}\Delta f_{\text{TR}}(y)/f_{\text{TR}}dy$. The formula for the large amplitude[26] was also tested but no significant difference was confirmed. In other words, the dithering amplitude of 81 pm was small enough for a direct-force-gradient detection at the tip-sample distance. The amplitude satisfying the condition of the small amplitude limit should be changed by the tip-sample distance and the interatomic distance of the sample

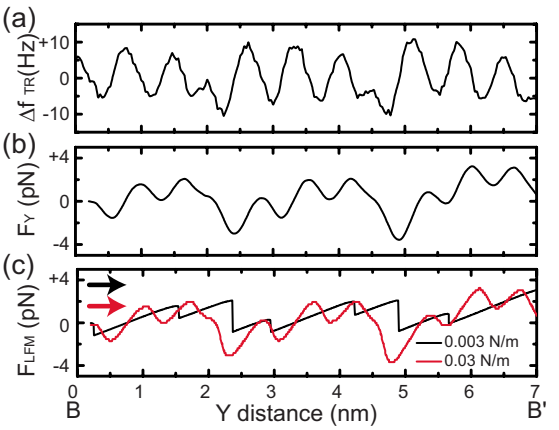

FIG. 4. (Color online) (a) Line profile of Δf_{TR} along B-B' in Fig. 3(a). $\bar{I}_t$=0.25 nA. (b) Converted lateral-force curve. (c) Simulated lateral force detected with k_{TR} of 0.003 and 0.03 N/m in static LFM.

surface. Figure 4(b) shows the calculated lateral-force curve.[14] Contrary to the case with the large amplitude, the frequency noises were averaged out in the conversion procedure and thereby an extremely small lateral force of less than 1 pN, which is 1 order of magnitude smaller than the detection limit in static LFM,[7] was detectable even at RT. The amount of the interaction force was so small that the deformation of the tip apex would be negligibly small. In other words the force curve shown in Fig. 4(b) can be regarded as the actual lateral interaction force without any influence of the stick-slip motion and the deformations of tip and sample.

In static LFM,[4] the frontmost atom of the tip is usually assumed to be in the repulsive interaction region but the friction measurement can, in principle, also be performed in the attractive interaction region if an appropriate force sensor to avoid the jump-to-contact instability is selected (i.e., pendulum sensor[27]). Here the experimentally detected lateral force is used to investigate tip movements in noncontact static LFM with a one-dimensional Tomlinson-type model. In the model the tip always stays at the minimum of the total potential V_{total} as[28]

$$V_{\text{total}}(Y_{\text{tip}}) = U_{ts}(Y_{\text{tip}}) + \frac{1}{2}k_{\text{TR}}(Y_s - Y_{\text{tip}})^2, \tag{3}$$

where Y_s and Y_{tip} are the positions of the cantilever support and the tip, respectively. By differentiating Eq. (3) the position of the tip can be obtained and so that the converted lateral-force ($F_Y = \partial U_{ts}/\partial Y_{\text{tip}}$) curve shown in Fig. 4(b) can be directly used for this simulation. Then, the lateral force in static LFM is obtained with $F_{\text{LFM}} = k_{\text{TR}}(Y_s - Y_{\text{tip}})$. Figure 4(c) shows simulated lateral-force curves with two different stiffnesses of 0.003 and 0.03 N/m. The tip movement was from left to right. The results were strongly affected by the lateral stiffness of the cantilever. In the case of $k_{\text{TR}} < 0.003$ N/m it is found that the stick-slip motion happens even at the attractive-force region. Therefore, the detected force in DLFM is the origin of the stick-slip motion. With a higher spring constant of 0.03 N/m, the tip traces the actual lateral force. However if the stiffness of the cantilever becomes comparable to that of the tip apex, the deformations of the tip apex would become non-negligible.[29] Nevertheless, since the detection sensitivity in static LFM has an inverse relationship with the spring constant ($\propto F_{\text{LFM}}/k_{\text{TR}}$), the detection of the actual force with a stiff-force sensor is not realistic. These criteria practically fail the actual lateral-force detection in static LFM. On the other hand, since the detection in DLFM is based on the frequency modulation technique, the relation between the stiffness of the tip apex and the lateral stiffness of the cantilever does not play a role. If the lateral force gradient is lower than these two stiffnesses, the actual force detection can be realized. As we demonstrated in this study, detections in the noncontact region can fulfill this criterion. Therefore, DLFM is an imperative technique for the actual lateral interaction.

IV. CONCLUSION

In this paper we demonstrated the successful direct detection of the lateral force gradient of less than 0.01 N/m while keeping atomic resolution with DLFM. The lateral-force spectroscopy revealed that the corresponding lateral force with the resolution of better than 1 pN indicates a possibility of detecting and controlling the noncontact atomic stick-slip motion. The theoretical simulations were in good agreement with the experimental results.

ACKNOWLEDGMENTS

This work was supported in part by JST-CREST and Japan Society for the Promotion of Science under Grant No. 20360022. The author (S.K.) would like to thank Alexis Baratoff for many discussions.

*shigeki.kawai@unibas.ch

[1] F. J. Giessibl, Science **267**, 68 (1995).
[2] T. R. Albrecht, P. Grütter, D. Horne, and D. Rugar, J. Appl. Phys. **69**, 668 (1991).
[3] B. N. J. Person, *Sliding Friction, Physical Principles, and Applications*, 2nd ed. (Springer-Verlag, Berlin, 2000).
[4] C. M. Mate, G. M. McClelland, R. Erlandsson, and S. Chiang, Phys. Rev. Lett. **59**, 1942 (1987).
[5] K. Miura, S. Kamiya, and N. Sasaki, Phys. Rev. Lett. **90**, 055509 (2003).
[6] J. Y. Park, D. F. Ogletree, M. Salmeron, R. A. Ribeiro, P. C. Canfield, C. J. Jenks, and P. A. Thiel, Science **309**, 1354 (2005).
[7] A. Socoliuc, E. Gnecco, S. Maier, O. Pfeiffer, A. Baratoff, R. Bennewitz, and E. Meyer, Science **313**, 207 (2006).
[8] W. A. Hofer, A. S. Foster, and A. L. Shluger, Rev. Mod. Phys. **75**, 1287 (2003).
[9] O. Pfeiffer, R. Bennewitz, A. Baratoff, E. Meyer, and P. Grütter, Phys. Rev. B **65**, 161403(R) (2002).
[10] F. J. Giessibl, M. Herz, and J. Mannhart, Proc. Natl. Acad. Sci. U.S.A. **99**, 12006 (2002).
[11] S. Kawai, S. Kitamura, D. Kobayashi, and H. Kawakatsu, Appl. Phys. Lett. **87**, 173105 (2005).
[12] A. Schwarz, H. Hölscher, S. M. Langkat, and R. Wiesendanger, AIP Conf. Proc. **696**, 68 (2003).
[13] M. Ternes, C. P. Lutz, C. F. Hirjibehedin, F. J. Giessibl, and A. J. Heinrich, Science **319**, 1066 (2008).
[14] Y. Sugimoto, T. Namikawa, K. Miki, M. Abe, and S. Morita, Phys. Rev. B **77**, 195424 (2008).
[15] M. A. Lantz, H. J. Hug, R. Hoffmann, P. J. A. van Schendel, P. Kappenberger, S. Martin, A. Baratoff, and H. J. Güntherodt, Science **291**, 2580 (2001).
[16] K. Takayanagi, Y. Tanishiro, M. Takahashi, and S. Takahashi, J. Vac. Sci. Technol. A **3**, 1502 (1985).
[17] R. Pérez, I. Štich, M. C. Payne, and K. Terakura, Phys. Rev. B **58**, 10835 (1998).
[18] N. Sasaki and M. Tsukada, Jpn. J. Appl. Phys., Part 1 **38**, 192 (1999).
[19] S. Kawai, D. Kobayashi, S. Kitamura, S. Meguro, and H.

Kawakatsu, Rev. Sci. Instrum. **76**, 083703 (2005).
[20] F. J. Giessibl, Rev. Mod. Phys. **75**, 949 (2003).
[21] S. Kawai, S. Kitamura, D. Kobayashi, S. Meguro, and H. Kawakatsu, Appl. Phys. Lett. **86**, 193107 (2005).
[22] N. Sasaki, S. Kawai, and H. Kawakatsu (unpublished).
[23] C. J. Chen, *Introduction to Scanning Tunneling Microscopy* (Oxford University Press, New York, 1993).
[24] K. D. Brommer, M. Needels, B. E. Larson, and J. D. Joannopoulos, Phys. Rev. Lett. **68**, 1355 (1992).
[25] N. Sasaki and M. Tsukada, Jpn. J. Appl. Phys., Part 2 **37**, L533 (1998).
[26] J. E. Sader and S. P. Jarvis, Appl. Phys. Lett. **84**, 1801 (2004).
[27] D. Rugar, R. Budakian, H. J. Mamin, and B. W. Chui, Nature (London) **430**, 329 (2004).
[28] E. Gnecco, R. Bennewitz, T. Gyalog, and E. Meyer, J. Phys.: Condens. Matter **13**, R619 (2001).
[29] A. Socoliuc, R. Bennewitz, E. Gnecco, and E. Meyer, Phys. Rev. Lett. **92**, 134301 (2004).